Single-Objective Topology Optimization and Experimental Validation of a VA Ferrite Plate for an SAE-Compliant WPT System

Giulio Poggiana, Wenjie Yuan, Riccardo Torchio, *Member, IEEE*, Francesco Lucchini, Vincenzo Cirimele, *Senior Member, IEEE*, Chunsen Tang, *Member, IEEE*, and Fabrizio Dughiero

***Abstract*— Ferrite plates are essential elements in wireless power transmission systems. Their presence is critical to achieving adequate magnetic coupling and minimizing the stray magnetic field. At the same time, reducing the volume of ferrite used in the vehicle assembly (VA) offers significant benefits in terms of cost and weight reduction. Topology optimization (TO) methods are particularly effective tools for applications like wireless power transfer (WPT), where the magnetic field is not confined to a well-defined volume, unlike in classical electrical machines. In the present work, the solid isotropic material with penalization (SIMP) method is used to achieve an optimized reduced-volume design of the VA ferrite plate of an SAE-compliant system. The optimized plate was manufactured and its performance was experimentally validated and compared to the original VA. The results show that the fabricated plate is able to maintain a mutual inductance reduction of less than 10% with a 55% reduction in material volume. The impact of the material reduction on the system's losses was also evaluated, revealing that the proposed solution results in a 3% increase in losses when tested on a 3.4-kW test bench.**

***Index Terms*— Electric vehicles, electromagnetic modeling, inductive power transfer, topology optimization (TO), wireless power transfer (WPT).**

I. Introduction

WIRELESS power transfer (WPT) is a rapidly advancing technology that enables devices to charge without physical connections to a power source, eliminating the limitations of traditional wired systems. This flexibility makes WPT systems a promising solution for a wide range of civil and industrial applications [1], [2], [3], [4], [5].

The growing interest in WPT is reflected in the rapid development of standards, with SAE J2954 [6] emerging as the most mature international reference [7]. It defines the implementation and operational requirements for static WPT systems and also proposes reference designs for the coils in the so-called ground assembly (GA) and vehicle assembly (VA). These design examples are based on ferrite tiles forming a continuous plate beneath each coil. Ferrite remains the most widely adopted material due to its high permeability and low losses at the typical operating frequencies and magnetic flux densities. However, it presents significant critical issues in terms of cost, weight, and fragility [8]. Moreover, its production entails carbon dioxide and greenhouse gas emissions. Although less impactful than other ferromagnetic materials, reducing ferrite use can enhance the sustainability of WPT systems by lowering their carbon footprint [9], [10], [11]. On the vehicle side, minimizing ferrite volume also contributes to reducing weight, supporting the vehicle's range extension [12].

Several works have addressed the optimization of the ferrite plates with the main objective of maximizing the magnetic coupling between the coils. Such optimizations are conducted through simple parametric sweeps, like in [13], [14], [15], and [16] or using optimization algorithms, like in [17], [18], and [19]. However, all of these works approach the optimization problem by starting from predefined shapes of ferrite tiles or bars and then repeating these shapes according to predetermined geometries and patterns that tend to trace the shape of the coils. Therefore, this approach relies on a qualitative assumption about the distribution of the magnetic field in the vicinity of the coils. This clearly limits the exploration of novel shapes that cannot be identified on the simple basis of experience.

Topology optimization (TO) can overcome such limitations. Indeed, this method aims to identify the optimal distribution of the material in a given domain by minimizing a cost function while accounting for constraints, without imposing a priori initial shapes or material distributions. Originally developed for solid mechanics engineering problems, TO has recently become attractive also in the design of electromagnetic devices [20], [21], [22], and some recent works have applied it to WPT applications. These works employ various TO approaches, which differ in the mathematical space where the design variables are defined. Some works adopt continuous type variables as in [23], [24], and [25], while others, such as [26], [27], [28], and [29], employ binary type variables.

Received 12 August 2025; revised 12 November 2025; accepted 28 December 2025. Date of publication 12 January 2026; date of current version 25 March 2026. This work was supported in part by Fondazione Cariverona "Bando Ricerca e Sviluppo 2023." *(Corresponding author: Vincenzo Cirimele.)*

Giulio Poggiana, Francesco Lucchini, and Fabrizio Dughiero are with the Department of Industrial Engineering, University of Padua, 35131 Padua, Italy (e-mail: giulio.poggiana@phd.unipd.it; francesco.lucchini@unipd.it; fabrizio.dughiero@unipd.it).

Wenjie Yuan and Chunsen Tang are with the School of Automation, Chongqing University, Chongqing 400044, China (e-mail: yuanwenjie@cqu.edu.cn; cstang@cqu.edu.cn).

Riccardo Torchio is with the Department of Industrial Engineering and the Department of Information Engineering, University of Padua, 35131 Padua, Italy (e-mail: riccardo.torchio@unipd.it).

Vincenzo Cirimele is with the Department of Electrical, Electronic, and Information Engineering, University of Bologna, 40136 Bologna, Italy (e-mail: vincenzo.cirimele@unibo.it).

Digital Object Identifier 10.1109/TTE.2026.3651913

The binary approach has the advantage of directly identifying where the material is placed. However, its discrete nature makes it computationally challenging. It may also result in designs with isolated patches of solid or empty material. Conversely, continuous methods distribute the material throughout the entire optimization domain, enabling gradient-based optimization algorithms. This allows for more efficient and robust optimization, though it does not provide a clear distinction between the presence or absence of material in the domain. [30].

TO-generated structures often have complex and irregular shapes that are difficult to manufacture. Thus, TO is frequently adopted as a preliminary design step to locate the distribution of the ferrite [23], [24]. In other cases, as also done in the present work, the shape obtained from the TO is simplified to allow for its manufacturability [25].

To date, few studies apply TO to the ferrite plate of an SAE-compliant WPT system, and even fewer validate designs experimentally under nominal power conditions. For instance, works [24], [29] focus on WPT for consumer electronics, while works [23], [26], [27] address electric vehicle applications but without full-power testing. Although work [25] reports 2-kW tests, the proposed system lacks SAE-compliance. Specifically, it assumes an axially symmetric coil configuration, which simplifies the analysis by considering only a single slice of the design domain and a lower frequency than that prescribed by the SAE standard. Similarly, work [28] includes tests at 10 kW using a non-SAE-compliant scaled-down coil pair based on the mixed use of ferrite and soft magnetic composites.

Compared to the reviewed studies, this work applies a continuous TO method to redesign the VA ferrite plate in an SAE-compliant 3.4-kW system made of the reference universal GA and VA provided by the standard. The plate obtained significantly reduces ferrite usage, resulting in a lighter assembly that can be directly substituted for the original plate while maintaining interchangeability. The magnetic characteristics of the new VA assembly are experimentally evaluated, and the performance of the system with the optimized plate is tested comparatively with the original system at the rated power. Finally, a comparative analysis between the proposed system and the reference configuration is conducted to evaluate their respective robustness against misalignment and their leakage magnetic flux density in the presence of the additional conductive shield and the vehicle mimic plate according to the recommendations of the SAE standard. To better highlight the contribution and novelty of this work, a quantitative comparison with the examined existing literature is summarized in Table I.

The remainder of this article is organized as follows. Section II describes the SAE-compliant WPT system adopted as the reference for this work. Section III outlines the basic concepts of the TO approach used. In Section IV, the numerical results from the performed optimization are presented and discussed. Section V details the experimental validation of the optimized VA, while Section VI compares the robustness against misalignment and the leakage magnetic flux density of the reference system and the optimized one, respectively.

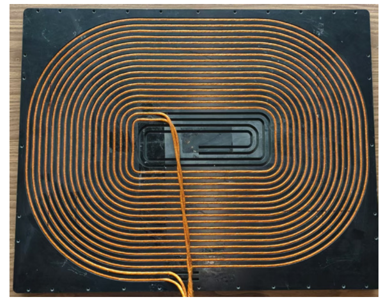

Fig. 1. GA coil of the system under study.

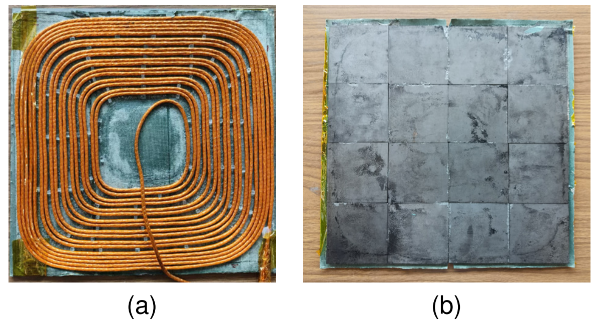

Fig. 2. (a) VA coil and (b) VA ferrite plate suggested by the SAE standard taken as reference for the TO.

The main outcomes of the work are finally summarized in Section VII.

II. Reference WPT System

The analysis in this article is based on a system that complies with the guidelines provided by the SAE J2954 standard. Specifically, on the transmitter side, an assembly is used that responds to the characteristics of the assembly referred to as the universal GA. As the name suggests, such a GA is designed to be cross-compliant among the different power classes defined by the SAE [7]. In fact, it serves as the transmitter-side reference for building the test bench for commercial VA validation. As illustrated in Fig. 1, the coil of this GA consists of eight turns, which are created by paralleling two Litz wire conductors with a net diameter of 4.7 mm. The spacing between these turns is 5 mm. The ferrite plate is positioned 4 mm beneath the coil and separated by a coil tray.

The VA is also constructed in accordance with one of the reference designs proposed by the SAE standard, as illustrated in Fig. 2. The coil comprises 16 turns of Litz wire, identical to that utilized in the GA. The fully filled ferrite plate is fabricated by bonding 16 tiles, each measuring 100 $\times$100 mm and with a thickness of 3 mm, made of KP95 ferrite. The ferrite used in this assembly has an initial relative magnetic permeability of 3500 and a saturation induction of 510 mT at 25 °C. The coil and ferrite plate are separated by a 2-mm layer of bakelite, which is covered with a Mylar sheet. This ferrite plate is not mechanically constrained to the coil, thereby allowing it to be replaced with a different plate without necessitating any alterations to the remainder of the assembly. An aluminum shield is positioned above the ferrite plate.

The main design parameters of the two assemblies are summarized in Table II together with the measured values of self-inductances and mutual inductance.

TABLE I
COMPARISON AMONG THE RECENT WORKS ON TO APPLIED TO WPT SYSTEMS

Work	TO approach	Transmitted power	Operating frequency	Experimental test at rated power	SAE compliance	Notes
[23]	Continuous	2.5 kW	85 kHz	✗	✗	
[24]	Continuous	∼ 10 W	100 kHz	✓	✗	
[25]	Continuous	2 kW	20 kHz	✓	✗	
[26]	Binary	7 kW	-	✗	✗	
[27]	Binary	-	85 kHz	✗	✗	
[28]	Binary	10 kW	85 kHz	✓	✗	Ferrite and SMC, no shield
[29]	Binary	-	100 kHz	✗	✗	
This work	Continuous	3.4 kW	85 kHz	✓	✓	Ferrite and shield

TABLE II
MAIN PARAMETERS OF THE REFERENCE GA AND VA ASSEMBLIES

Item	Value
GA ferrite plate size	650 mm × 500 mm
GA ferrite thickness	10 mm
VA ferrite plate size	350 mm × 350 mm
VA ferrite thickness	3 mm
Ferrite relative permeability	3500
VA aluminum shield size	350 mm × 350 mm
VA aluminum shield thickness	5 mm
GA coil number of turns	8 turns (2 wires in parallel)
VA coil number of turns	16
Litz wire characteristics	0.1 × 1200
Rated air-gap	180 mm
GA coil self-inductance	47.9 μH
VA coil self-inductance	125 μH
Mutual inductance	11.1 μH

The TO process is intended to replace the ferrite plate in Fig. 2(b) with a lighter plate to obtain a VA that is interchangeable with the previous one.

The current version of the SAE standard does not provide specific guidelines on interchangeability. For this reason, the verification criterion adopted in this study is based on the criteria for magnetic interoperability, as defined in the SAE standard [6, Appendix K]. Since the number of turns of the GA and the VA remains constant, the interchangeability of the two VAs is considered verified in this work if the variation in the mutual inductance value with respect to the same GA remains within a deviation of no more than 10%.

III. ADOPTED TO APPROACH

TO has recently gained increasing interest in various electromagnetic applications due to its unique ability to find the optimal distribution of a given amount of material within a design domain (D). This capability is particularly valuable in applications where the optimal arrangement of material within the device is unknown. In particular, applying this technique to the design of electromagnetic components with a reduced material volume can yield performances comparable to those of the full-volume case. In this section, the TO concept is briefly recalled; the interested reader can find detailed information in [30] and [31].

TO is formulated as a constrained minimization problem

$$\min f(\theta) \quad \text{under} \quad G(\theta) \leq 0 \tag{1}$$

where θ is the design variable (also called density), f is the objective function, and G is the constraint. A natural constraint appearing in TO problems is the final amount of material with a prescribed property that must be kept below a given value. In particular, a constraint on the ratio between the actual volume of material distributed in D, i.e., $V(\theta)$, and the entire volume of D, i.e., V_D, is applied

$$\frac{V(\theta)}{V_D} - V_{\text{frac}} \leq 0 \tag{2}$$

where V_{frac} is the target fraction of material. Without this constraint, the trivial optimal solution would often be to fill the entire domain with material, which is generally neither meaningful nor practical. Therefore, imposing a volume constraint is a natural and essential part of TO formulations and is widely used across fields, including structural mechanics and electromagnetics [22], [32], [33]. The minimization problem (1) is typically solved with deterministic iterative optimization strategies, where the sensitivity of the objective function with respect to the design variable is computed to iteratively update the material distribution within the domain [31]. Fig. 3 gives a conceptual representation of the logic of the TO algorithm.

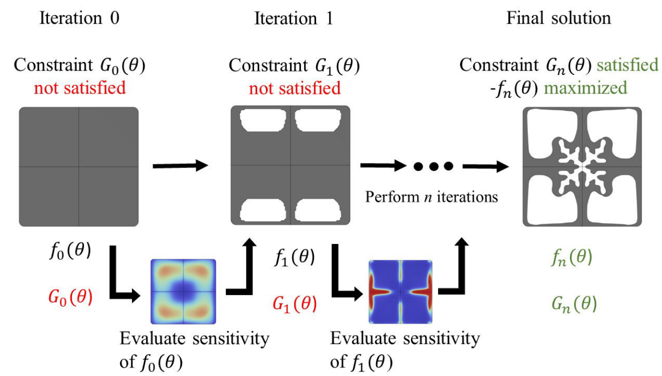

Fig. 3. Conceptual representation of the TO iteration process.

In this study, the solid isotropic material with penalization (SIMP) approach [31] is used to find the optimal distribution of the relative magnetic permeability within the optimization domain D corresponding to the ferrite of the VA.

Given a subdivision of D into finite elements, the TO assigns to each element of the mesh a density $0 \leq \theta_i \leq 1$ such that the material property $\mu_{r,i}$ assigned to the ith element is reconstructed through the following material interpolation scheme (MIS):

$$\mu_{r,i} = \mu_{r,\text{air}} + \left(\mu_r - \mu_{r,\text{air}}\right)\theta_i^{\alpha} \tag{3}$$

where $\mu_{r,\text{air}}$ and μ_r are the relative permeability of air and ferrite, respectively, and α is the penalization parameter. The correspondence between θ_i and the distributed material can be argued from Fig. 4. To clarify, when $\theta_i = 0$, the relative

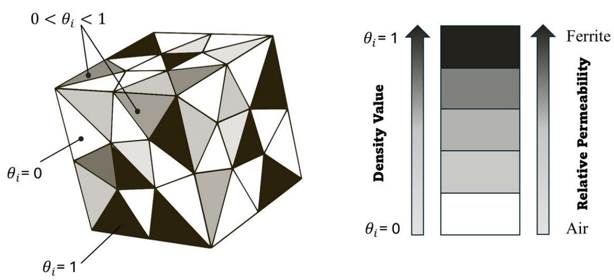

Fig. 4. Conceptual representation of the SIMP approach.

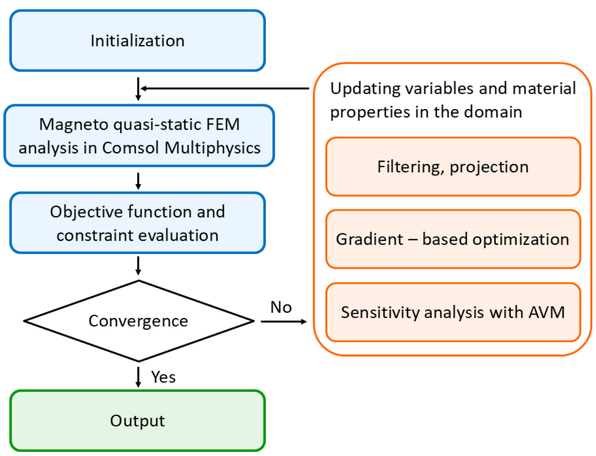

Fig. 5. Flowchart of TO based on SIMP method presented in this work.

permeability of the element is 1, indicating that the equivalent material can be assumed to be air. Conversely, when $\theta_i = 1$, the equivalent permeability corresponds to μ_r, indicating that the material is ferrite.

In this work, the TO process is carried out using the finite element method (FEM). Specifically, the optimization module of the commercial FEM software COMSOL has been employed, where the SIMP approach is implemented. The TO procedure follows the flowchart illustrated in Fig. 5. The optimization algorithm adopted is the method of moving asymptotes (MMA), which is particularly tailored for solving this kind of problem [34].

Optimizing the GA and VA of WPT systems is, in general, a multiobjective optimization problem, where several aspects are considered as objective functions [18], [35]. It is worth noting that, due to the high dimensionality of TO and its reliance on gradient-based methods, implementing a full multiobjective framework remains challenging and is an active research topic in the field [36], [37]. In this article, a single-objective optimization with constraints is therefore adopted, and the resulting topology is evaluated against all relevant key performance indicators to ensure a comprehensive a posteriori assessment. The objective of the optimization problem is to maximize the mutual inductance M while constraining the volume fraction of the ferrite VA plate to remain under a predetermined threshold.

In the SIMP approach, since the design variable θ_i is continuous, "grayscales" arise; for intermediate values of θ_i, the equivalent relative permeability does not correspond strictly to either air or ferrite. Cutting the grayscales at the end of the optimization process is required since, for the physical realization of the device, it is necessary to decide whether or not to insert the material. In this work, an accurate choice of the parameters [e.g., α in (3)] and numerical techniques, such as the Helmholtz filter and the hyperbolic tangent projection, were applied at each iteration to reduce the grayscale phenomenon as discussed in [30] and [38]. Specifically, in the Helmholtz filtering stage, the filter radius was set equal to the maximum element size of the mesh, while for the hyperbolic tangent projection, a projection slope of $\beta = 8$ and a projection point of $\theta_b = 0.5$ were used. Finally, a value of $\alpha = 7$ was adopted for the MIS. Furthermore, at the end of the optimization, all elements with $\theta_i > 0.5$ were assigned to ferrite.

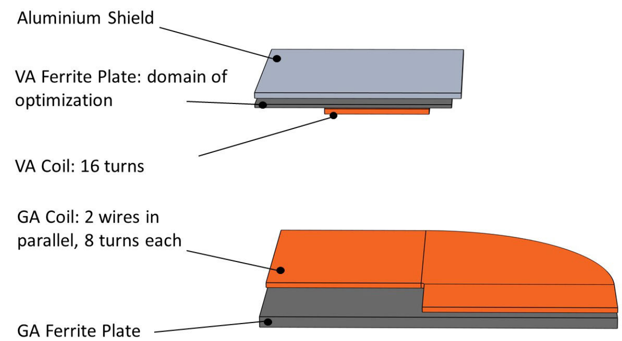

Fig. 6. Geometry implemented to perform the TO simplified through symmetry strategy and massive conductor equivalent description.

Since TO involves a large number of variables, equal to the number of mesh elements in the optimization domain, it is important to employ strategies that allow for reducing the computational cost while maintaining accurate results when creating the FEM model of the device under study. In the FEM model, a simplified massive conductor equivalent description is used for both the receiver and transmitter coils. This geometric simplification enables the use of a symmetry strategy where the simulation is performed on only a quarter of the total geometry, and symmetry is subsequently applied to reflect the results across the entire structure.

The geometry of the model implemented to perform the optimization is shown in Fig. 6.

The problem is treated as a magneto quasi-static problem and solved via the magnetic vector potential $\mathbf{A}$ formulation. Therefore, the mutual inductance, which is the objective function of the optimization problem, is computed from the magnetic vector potential through the relationship

$$M = \frac{\int_{V_{\mathrm{VA}}} \mathbf{A} \cdot \mathbf{v}\, dV}{S_{\mathrm{VA}} I_{\mathrm{GA}}} \tag{4}$$

where the volume integral is performed along the VA coil, $\mathbf{v}$ is a versor indicating the winding direction, S_{VA} is the section of the massive conductor that simplifies the VA coil, and I_{GA} is the current flowing in the transmitter coil that generates the magnetic field assumed equal to 1 A for the computation of M. This current value is chosen to avoid introducing nonlinearities into the model. Consequently, magnetic saturation is addressed through a constraint on the normalized maximum magnetic

TABLE III
OBTAINED VALUES OF MUTUAL INDUCTANCE FOR DIFFERENT CONSTRAINED FRACTIONS OF VOLUME

Fraction of Volume	M	Reduction in M
25%	9.3 μH	16%
40%	10.5 μH	5%
55%	10.8 μH	2%
70%	11.0 μH	0.4%

flux density. If this constraint is violated, the optimization algorithm adjusts the magnetic core geometry, avoiding saturation while maintaining the linearity of the overall problem. To avoid nonlinearities, the relative magnetic permeability of the ferrite is also assumed constant with respect to both temperature and frequency.

Preliminarily to its use for the TO, the model was validated by obtaining a mutual inductance value of 11.06 μH that deviates from the measured value by only 0.4%.

IV. TO RESULTS

Equation (2) outlines the TO problem as a constrained one, where the applied constraint is the ratio between the actual volume of material distributed in D and the entire volume of D. To investigate the effects of different material distributions, the optimization process in this work has been performed by imposing different maximum allowable volume fractions for the material.

The optimization results, along with the final proposed design, are detailed in Section IV-A. Additionally, the methodology used for estimating and analyzing losses in the optimized plate is presented in Section IV-B. The optimization was performed on a workstation equipped with an Intel Xeon processor (16 cores, 3.10 GHz) and 128 GB of RAM. The total computation time was approximately 10 h and 30 min for each imposed material fraction case.

A. TO Results

The resulting shapes for the different maximum amounts of material imposed as constraints in the TO are finally presented in Fig. 7, while the corresponding values of M are summarized in Table III. It is worth noting that the shapes obtained cannot be correlated with any information that could be evaluated a priori. This characteristic highlights the strength of TO as a powerful tool for identifying entirely new and nonintuitive optimal geometries.

From Table III, it can be observed that reducing the material volume by 30% results in a negligible reduction in mutual inductance. Furthermore, it can be observed that it is possible to use half, or even less, of the original material volume and still achieve acceptable performance in terms of mutual inductance.

As discussed in Section II, the optimized VA is considered interchangeable with the original VA if their mutual inductance with respect to the GA remains the same within a tolerance of 10%. Among the identified solutions, the one that allows for compliance with this constraint by achieving the greatest volume reduction is the solution with a ferrite volume fraction of 40%, which results in a mutual inductance reduction of about 5%.

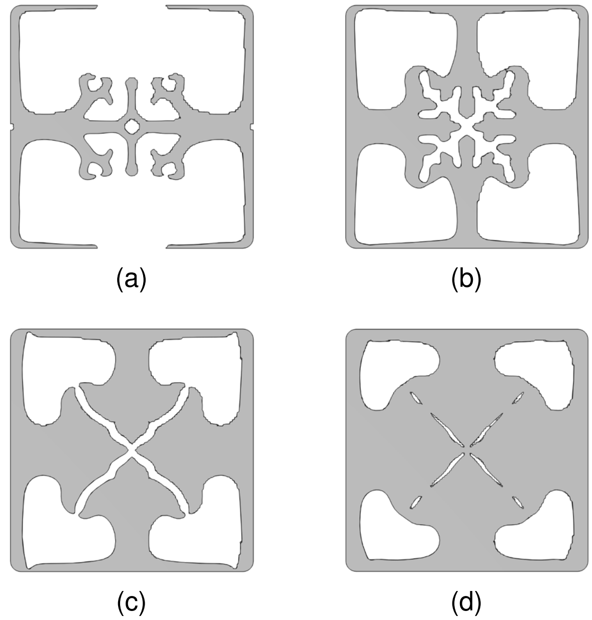

Fig. 7. VA ferrite after TO with a material fraction of volume of (a) 25%, (b) 40%, (c) 55%, and (d) 70%.

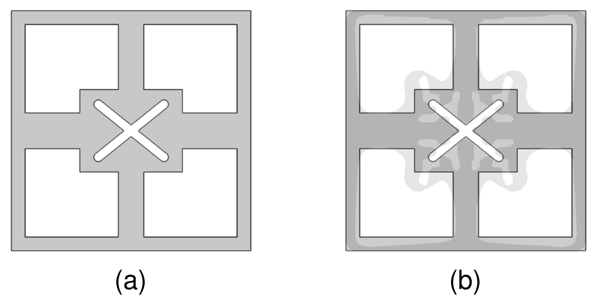

Fig. 8. (a) Optimized VA ferrite plate with simplified shape and (b) comparison between the shape resulting from TO and simplified one.

It is evident that the final shape of this VA plate appears critical from a fabrication point of view, as it exhibits uneven geometries with jagged edges. For this reason, this geometry is simplified as shown in Fig. 8(a). To make the simplification introduced better appreciable, the simplified geometry is superimposed in transparency on the geometry obtained from the TO process in Fig. 8(b). It is possible to appreciate how the simplified geometry aligns with the original one. However, it is also evident that the proposed final plate presents a slightly increased volume of ferrite compared to the original TO solution, along with a modified material distribution in the central region. In particular, the volume of the simplified plate is about 45% of the full ferrite plate. Hence, the proposed solution results in a reduction in ferrite of approximately 55% compared to the starting SAE-compliant VA plate. The numerical evaluation of the mutual inductance related to this final shape provides a value of 10.20 μH, which is slightly lower than the value obtained for the nonsimplified geometry due to the manufacturing simplifications introduced.

By analyzing the optimized shape obtained through TO, it can be observed that when the available material volume is significantly constrained, the TO algorithm tends to prioritize the creation of a low magnetic impedance path from the center to the outer edges of the plate, rather than directly across the windings as might be intuitively expected. This results in the "arms" of the structure. When the material is removed from a region, this indicates that the area does not contribute effectively to guiding the magnetic flux and is therefore more likely to be excluded during optimization. This behavior is particularly evident in the central region, where the magnetic flux density is nearly zero and does not influence the mutual inductance, as also demonstrated in previous studies [13]. This ultimately leads to the formation of the central cross.

B. Losses' Estimation Methodology

The reduction in mutual inductance, albeit slight, and the reduction in the volume of material in the VA ferrite plate can result in a reduction in the efficiency of the WPT system. In fact, a lower M implies an increase in the GA coil current to maintain the same transferred power, which increases Joule losses in the coil. At the same time, the reduction in ferromagnetic material decreases the flux-carrying cross section. This can result in increased magnetic flux density in the ferrite and a possible consequent increase in losses within the ferrite material itself. Therefore, it is important to take loss aspects into consideration in order to ensure a comprehensive and systematic evaluation of the optimization outcome.

The losses in the GA and VA assemblies can be categorized into coil losses, losses in the ferromagnetic materials, and losses in the aluminum shields. Given that this work focuses on analyzing the effects of material reduction on the ferrite plate, particular attention has been placed on isolating and estimating the losses specifically associated with the ferrite. However, experimentally separating the contributions of the plate losses from the others is very challenging, as the current density distribution in the conductors is influenced by the surrounding materials.

To achieve this, the ferrite plate losses were estimated using the Steinmetz model, which relies on simulated magnetic flux density values. In such systems, the currents in the coils, particularly on the receiver side, can be assumed sinusoidal with a good degree of accuracy [39]. Therefore, no advanced ferromagnetic loss calculation methods are required [40], and the use of the Steinmetz model is fully justified.

The core loss was then evaluated numerically by integrating over the volume of each core the loss density p_{core}, expressed in W/m^3 and defined according to the Steinmetz equation

$$p_{\text{core}} = k \cdot f^{\alpha} \cdot \hat{B}^{\beta} \quad (5)$$

where the parameters k, α, and β are the Steinmetz parameters of the core material; f is the frequency expressed in hertz; and $\hat{B}$ is the peak value of the magnetic flux density, expressed in tesla. The value of $\hat{B}$ was obtained by imposing the rms value of the first harmonic of the coil currents measured during the full-power test. For the KP95 ferrite used in this work, the parameters are derived from the core loss behavior provided in the ferrite manufacturer's datasheet. The adopted parameters are: $k = 1.97$, $\alpha = 1.5$, and $\beta = 3.22$.

The losses in the aluminum shield were also evaluated numerically by simulating the induced power dissipated in the shield when the coils were supplied with the currents measured during the full-power test. Regarding the coil losses, the resistances of the coils were measured using an LCR meter with a measurement current limited to 1 mA at 85 kHz. This limited value of the current allowed for considering the effect of the ferrite on the current density distribution, but, at the same time, to minimize the induction value in the ferrite and therefore neglect its losses. The resistance values obtained through the measurement were multiplied by the square of the rms values of the currents measured in the coils during full-power tests, thus obtaining values representative of Joule losses.

The outcome of these evaluations is presented in direct comparison with the experimental efficiency results in Section V.

Fig. 9. Manufactured VA ferrite plate for the SAE-compliant WPT system.

TABLE IV
COMPARISON BETWEEN SIMULATED MUTUAL INDUCTANCE AND MEASURED ONE

	Simulated M	Measured M	Relative error
Reference plate	11.06 μH	11.10 μH	0.4%
Optimized plate	10.20 μH	10.23 μH	0.3%
Difference in M	8%	8%	-

TABLE V
PERFORMANCE TEST AT 3.4- kW AND EFFICIENCY EVALUATION

Parameter	Reference plate	Optimized plate
Output Power	3.43 kW	3.39 kW
Input Power	3.70 kW	3.78 kW
R_{GA}	50 mΩ	50 mΩ
R_{VA}	150 mΩ	170 mΩ
I_{GA}	30 A	33.75 A
I_{VA}	19.6 A	19.4 A
Total measured losses	270 W	390 W
Evaluated coils losses	102.6 W	121 W
Simulated ferrite losses	3.15 W	57 W
Simulated shield losses	1.1 W	5 W
DC-DC Efficiency	93%	90%

V. EXPERIMENTAL VALIDATION

The simplified geometry obtained from the TO process was applied to the construction of the ferrite plate shown in Fig. 9. Most of the structure was obtained by assembling standard elements, while the more complex part was creating the cut in the center, which was done using waterjet cutting, a rapid process involving minimal material waste. This optimized plate was compared through various tests and measurements to the original plate of the system described in Section II.

The first comparative test was conducted by measuring the mutual inductance value through an LCR meter measurement. The result was also related to the values obtained through

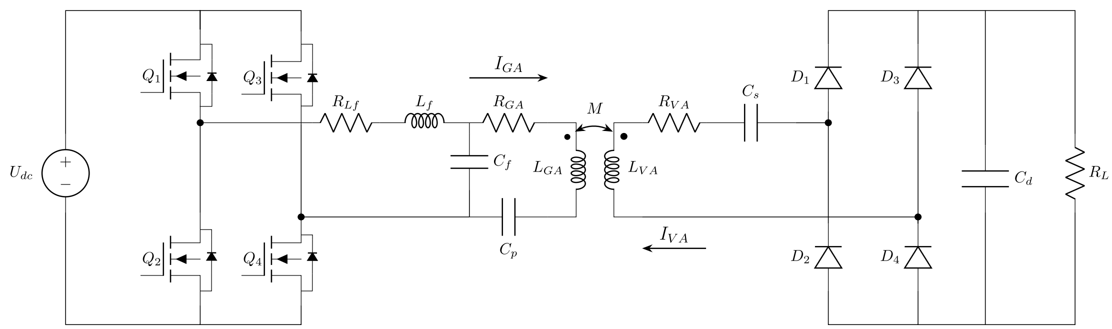

Fig. 10. Equivalent circuit representation of the WPT system under test.

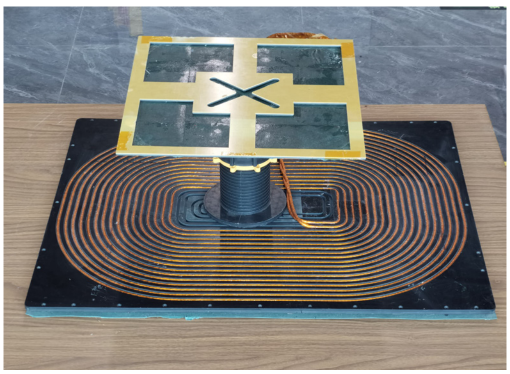

Fig. 11. Optimized SAE-compliant proposed system. The aluminum shield is not present to better appreciate the shape of the ferrite plate.

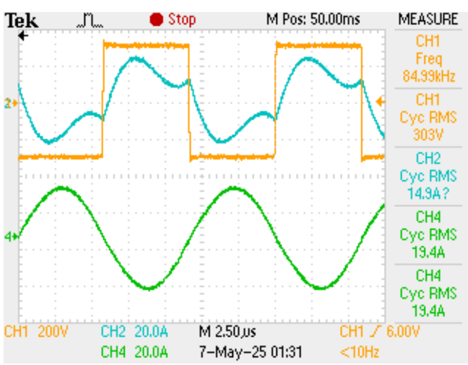

(a)

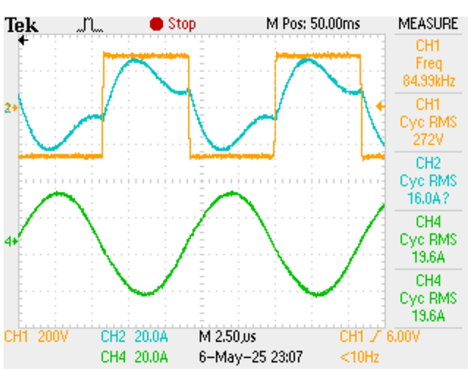

(b)

Fig. 12. Source dc/ac converter output voltage (orange trace), current (light blue trace), and VA coil current (green trace) waveforms for the system with (a) reference plate and (b) optimized one.

the numerical model and reported in Table IV. The experimental results show good agreement with the numerically simulated values. Minor discrepancies may be due as much to the approximation introduced for conductor modeling as to machining tolerances and tolerances on coil placement during measurements. Additionally, the experimental measurements confirm that the variation in mutual inductance M remains well below 10%, confirming the interchangeability of the two assemblies.

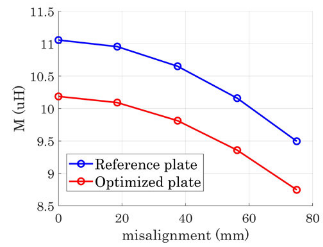

(a)

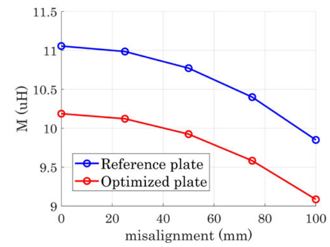

(b)

Fig. 13. Measured value of M as a function of the misalignment along (a) X-axis and (b) Y-axis.

Having verified the compliance of the optimized VA plate, the two assemblies were deployed in the same WPT system and operated to obtain the same output power of 3.4 kW. The operating frequency in both cases remained unchanged and equal to 85 kHz by modifying only the compensation capacitors connected to the VA coil. The system employs an LCC compensation topology for the GA and a series compensation topology for the VA. The LCC-S compensation was chosen since it offers advantages in terms of control of the charging process and ensures inherent operational safety even in the case of sudden and unexpected disconnection of the load [41]. However, it is worth noting that the methodology used in this work, which focuses solely on the mutual coupling between the coils, remains valid regardless of the compensation topology adopted.

The transmitted power is regulated by modifying only the dc voltage of the source dc/ac converter. A simplified scheme of the resonant system with LCC-S topology is drawn in Fig. 10.

The assembly of the GA coil, which remains unchanged, and the optimized assembly can be seen in Fig. 11. The dc/ac output voltage and current waveforms for both the system with the reference plate and the optimized system are shown in Fig. 12. It can be observed that the difference in M between the two systems necessitates an adjustment of the source voltage.

The obtained results are presented in Table V, where I_{GA} and I_{VA} are the measured rms current values in the coils. Efficiency was calculated as the ratio of the power measured at the system input dc bus to the dc power output of the system,

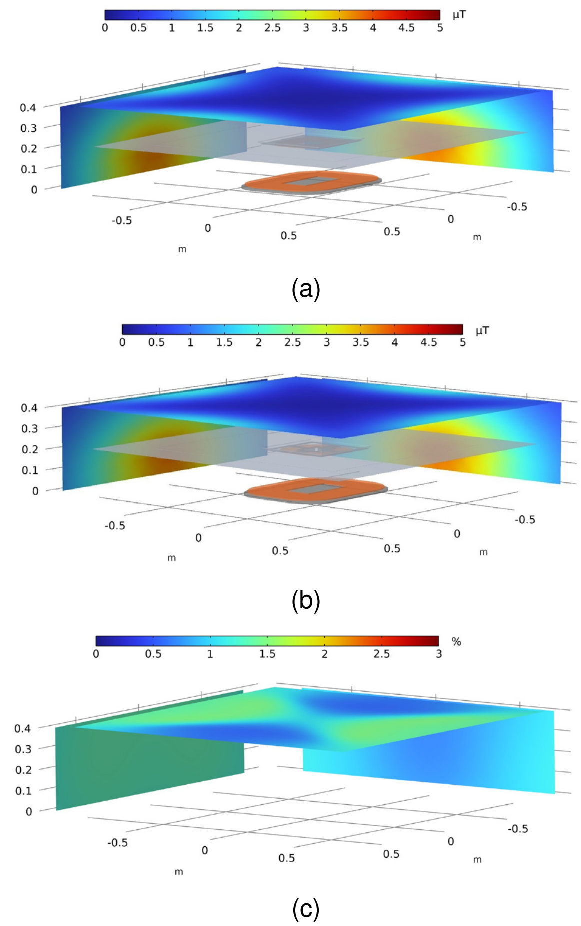

Fig. 14. Leakage B-field for the system with (a) reference plate, (b) optimized one, and (c) relative difference between the two.

while the total losses were derived by subtracting the output power from the input power. Along with the efficiency values, the losses in the coils, ferrite plates, and aluminum shields, calculated as described in Section IV-B, are reported.

Experimental results show that the use of the optimized plate does indeed result in a 3% reduction in efficiency. However, this reduction in efficiency corresponds to a volume (and therefore weight) reduction of 55%. The results obtained through numerical models indicate precisely how the increase in losses is related to the reduction in material cross section, leading to an increase in magnetic flux density compared with the starting configuration with a full ferrite plate. At the same time, the 8% reduction in mutual inductance is compensated for by an increase in current on the primary coil, which also causes an increase in losses in the conductor. In an engineered application, it is possible to operate iteratively, i.e., gradually relax the volume fraction imposed for the TO and evaluate the effect on losses until a suitable tradeoff is found.

VI. Misalignment and Leakage Magnetic Flux Density Assessment

Once the simulation results were validated and the power transmission capability of the proposed system was confirmed, further evaluations were required to assess the system's compliance with SAE standard requirements. Therefore, an additional analysis of the proposed system under misalignment conditions is presented in Section VI-A, while a comparative analysis of the leakage magnetic flux density (B-field) is provided in Section VI-B.

A. Misalignement Analysis

In accordance with the SAE standard, which specifies a maximum misalignment of 75 mm along the X-axis and 100 mm along the Y-axis [6], the measurements of mutual inductance were carried out at five equally spaced positions along each direction, ranging from 0 to the respective maximum misalignment values. The measured values of M as a function of misalignment along the two axes are presented in Fig. 13, for both the reference plate and the optimized one.

It is important to note that the adoption of the optimized ferrite plate does not lead to a more rapid decrease in M under misalignment conditions. The difference in M between the reference plate and the optimized configuration remains approximately constant across the tested misalignment range.

B. Leakage B-Field Analysis

A further comparison between the reference plate and the optimized one deals with the evaluation of the leakage magnetic flux density (B-field). According to the SAE standard [6], the B-field must be evaluated at a distance of 20 cm from the vehicle chassis (i.e., any conductive or ferromagnetic element) to avoid edge effects. The application is considered compliant if the field remains below the reference level of 27 μT.

In this study, the vehicle is emulated through the steel vehicle mimic plate defined in the test bench reported in the SAE standard. This plate has dimensions 1.5 $\times$ 1.5 m and is placed directly above the aluminum shield as visible in Fig. 14.

Fig. 14 reports the distributions of the B-field evaluated over three perpendicular observation planes positioned at the prescribed distance from the mimic plate. The relative difference between the case with the reference plate and the one with the optimized plate is reported in Fig. 14(c). This figure demonstrates that the adoption of the optimized ferrite plate has only a marginal effect on the leakage magnetic flux density. The reference level of 27 μT prescribed by the standard is never exceeded in any of the observation planes for both cases with reference and optimized plate, allowing both solutions to be considered compliant.

VII. Conclusion

This article proposed and analyzed an innovative design of the ferrite plate of an SAE-compliant system obtained through the application of a dedicated topological optimization technique. The aim was to achieve a design with as little system weight as possible while maintaining compliance with the design proposed by the standard and full interchangeability with the latter.

The proposed design was developed using the SIMP approach, framing the problem as a constrained optimization task. The objective function aimed to maximize the mutual inductance, while the constraints ensured the ferrite volume remained within a predefined limit.

A novel configuration has been derived from the TO and subsequently manufactured for experimental validation.

A 3.4-kW test bench has been implemented to validate the numerical results and compare the novel solution with the initial design. The work's outcomes demonstrate that an optimized material reduction of approximately 55% led to only an 8% decrease in mutual inductance, highlighting the effectiveness of the proposed approach in maintaining system performance while significantly reducing material usage. The experimental results at the rated power level demonstrate that a 55% reduction in ferrite material results in a 3% decrease in dc–dc efficiency. This difference is due to the increase in current in the transmitter coil caused by the reduction in mutual inductance and the increase in losses in the ferrite due to the reduction in the cross section of the ferrite, which causes an increase in the induction level.

The optimized system has also been compared with the reference configuration in terms of robustness against misalignment and leakage magnetic flux density, following the assessment guidelines prescribed by the SAE standard. These comparative analyses demonstrated that the adoption of the optimized ferrite plate does not result in a more rapid decrease in mutual inductance under misalignment conditions and has only a marginal effect on the leakage magnetic flux density, which remains well below the reference limit specified by the standard.

Finally, it is worth mentioning that the primary objective at this stage of the research was to experimentally validate the numerical results of the TO. Thus, the manufactured ferrite core was designed to replicate as closely as possible the shape obtained from the optimization algorithm. Future research will be aimed at exploring solutions to take into account potential industrial cost constraints.

REFERENCES

[1] V. Cirimele, F. Freschi, and M. Mitolo, "I charge, therefore I drive: Current state of electric vehicle charging systems," *IEEE Power Energy Mag.*, vol. 21, no. 6, pp. 91–97, Nov. 2023.

[2] T. Campi, S. Cruciani, F. Palandrani, V. De Santis, A. Hirata, and M. Feliziani, "Wireless power transfer charging system for AIMDs and pacemakers," *IEEE Trans. Microw. Theory Techn.*, vol. 64, no. 2, pp. 633–642, Feb. 2016.

[3] G. Buja, M. Bertoluzzo, and K. N. Mude, "Design and experimentation of WPT charger for electric city car," *IEEE Trans. Ind. Electron.*, vol. 62, no. 12, pp. 7436–7447, Dec. 2015.

[4] V. Cirimele, R. Mandrioli, R. Torchio, G. Gentile, F. Giulietti, and G. Grandi, "Design considerations on modular WPT charging systems for drones in civil applications," in *Proc. Int. Conf. Clean Electr. Power (ICCEP)*, Jun. 2023, pp. 452–457.

[5] D. Patil, M. K. McDonough, J. M. Miller, B. Fahimi, and P. T. Balsara, "Wireless power transfer for vehicular applications: Overview and challenges," *IEEE Trans. Transport. Electrific.*, vol. 4, no. 1, pp. 3–37, Mar. 2018.

[6] *Wireless Power Transfer for Light-Duty Plug-In/Electric Vehicles and Alignment Methodology*, Standard International SAE J2954, 2019.

[7] V. Cirimele, F. Freschi, and L. Zhao, "Critical comparative review of international standards on wireless charging for light-duty electric vehicles," *IEEE Trans. Ind. Appl.*, vol. 60, no. 5, pp. 7403–7412, Sep. 2024.

[8] M. G. S. Pearce, G. A. Covic, and J. T. Boys, "Robust ferrite-less double d topology for roadway IPT applications," *IEEE Trans. Power Electron.*, vol. 34, no. 7, pp. 6062–6075, Jul. 2019.

[9] P. Gómez, D. Elduque, C. Pina, and C. Javierre, "Influence of the composition on the environmental impact of soft ferrites," *Materials*, vol. 11, no. 10, p. 1789, Sep. 2018.

[10] A. Amato et al., "Life cycle assessment of rare Earth elements-free permanent magnet alternatives: Sintered ferrite and Mn–Al–C," *ACS Sustain. Chem. Eng.*, vol. 11, no. 36, pp. 13374–13386, Sep. 2023.

[11] P. K. Surarapu, G. Mallela, and N. Ramu, "Life cycle assessment of samarium ferrite materials for electronic devices," *Mater. Today, Proc.*, vol. 52, pp. 1589–1593, Jan. 2022.

[12] M. Mruzek, I. Gajdáč, L. Kučera, and D. Barta, "Analysis of parameters influencing electric vehicle range," *Proc. Eng.*, vol. 134, pp. 165–174, Jan. 2016.

[13] M. Bensetti, K. Kadem, Y. Pei, Y. Le Bihan, E. Labouré, and L. Pichon, "Parametric optimization of ferrite structure used for dynamic wireless power transfer for 3 kW electric vehicle," *Energies*, vol. 16, no. 14, p. 5439, Jul. 2023.

[14] I. Casaucao, A. Triviño, and A. Delgado, "Ferromagnetic design of coils considering misalignment effects for a SAE J2954-compliant EV wireless charger," *IEEE Access*, vol. 12, pp. 163978–163987, 2024.

[15] R. Bosshard, J. Muhlethaler, J. W. Kolar, and I. Stevanovic, "Optimized magnetic design for inductive power transfer coils," in *Proc. 28th Annu. IEEE Appl. Power Electron. Conf. Expo. (APEC)*, Long Beach, CA, USA, Mar. 2013, pp. 1812–1819.

[16] H. Zhuang, W. Wang, and G. Yan, "Ferrite concentrating and shielding structure design of wireless power transmitting coil for inductively coupled capsule robot," *IEEE Trans. Biomed. Circuits Syst.*, vol. 17, no. 1, pp. 45–53, Feb. 2023.

[17] S. Shimokawa et al., "Fast 3-D optimization of magnetic cores for loss and volume reduction," *IEEE Trans. Magn.*, vol. 54, no. 11, pp. 1–4, Nov. 2018.

[18] R. Bosshard and J. W. Kolar, "Multi-objective optimization of 50 kW/85 kHz IPT system for public transport," *IEEE J. Emerg. Sel. Topics Power Electron.*, vol. 4, no. 4, pp. 1370–1382, Dec. 2016.

[19] V. Bertolini, F. Corti, M. Intravaia, A. Reatti, and E. Cardelli, "Optimizing power transfer in selective wireless charging systems: A genetic algorithm-based approach," *J. Magn. Magn. Mater.*, vol. 587, Dec. 2023, Art. no. 171340.

[20] K. Watanabe, T. Suga, and S. Kitabatake, "Topology optimization based on the ON/OFF method for synchronous motor," *IEEE Trans. Magn.*, vol. 54, no. 3, pp. 1–4, Mar. 2018.

[21] Y. Otomo and H. Igarashi, "Topology optimization using Gabor filter: Application to synchronous reluctance motor," *IEEE Trans. Magn.*, vol. 57, no. 6, pp. 1–4, Jun. 2021.

[22] G. Poggiana, M. Zorzetto, F. Lucchini, R. Torchio, M. Forzan, and F. Dughiero, "Topology optimization of a nonlinear ferrite core for induction heating in injection molding," *COMPEL Int. J. Comput. Math. Electr. Electron. Eng.*, vol. 44, no. 3, pp. 303–313, Dec. 2024.

[23] Y. Pei, L. Pichon, Y. L. Bihan, and M. Bensetti, "SIMP-method topology optimization of ferrite structures in inductive power transfer systems," *IEEE Trans. Electromagn. Compat.*, vol. 65, no. 6, pp. 1744–1750, Dec. 2023.

[24] C. Lee, "Topology optimization of the transmitter ferrite and receiver coil for minimizing the weight of the wireless-charging portable devices," *IEEE Trans. Ind. Electron.*, vol. 71, no. 10, pp. 12192–12201, Oct. 2024.

[25] M. Hu and U. K. Madawala, "Magnetic structure design in IPT systems based on topology optimization," *IEEE Trans. Transport. Electrific.*, vol. 11, no. 2, pp. 5374–5386, Apr. 2025.

[26] F. Lucchini, R. Torchio, P. Bettini, and F. Dughiero, "TopIE: An integral equation tool for topology optimization in electromagnetics," *IEEE Trans. Antennas Propag.*, vol. 72, no. 1, pp. 683–692, Jan. 2024.

[27] Y. Otomo and H. Igarashi, "A 3-D topology optimization of magnetic cores for wireless power transfer device," *IEEE Trans. Magn.*, vol. 55, no. 6, pp. 1–5, Jun. 2019.

[28] B. S. Gu, T. Dharmakeerthi, S. Kim, M. J. O'Sullivan, and G. A. Covic, "Optimized magnetic core layer in inductive power transfer pad for electric vehicle charging," *IEEE Trans. Power Electron.*, vol. 38, no. 10, pp. 11964–11973, Oct. 2023.

[29] B.-G. Choi, E. S. Lee, and Y.-S. Kim, "Optimal structure design of ferromagnetic cores in wireless power transfer by reinforcement learning," *IEEE Access*, vol. 8, pp. 179295–179306, 2020.

[30] F. Lucchini, R. Torchio, V. Cirimele, P. Alotto, and P. Bettini, "Topology optimization for electromagnetics: A survey," *IEEE Access*, vol. 10, pp. 98593–98611, 2022.

[31] O. Sigmund and K. Maute, "Topology optimization approaches: A comparative review," *Struct. Multidisciplinary Optim.*, vol. 48, no. 6, pp. 1031–1055, Dec. 2013.

[32] J. D. Deaton and R. V. Grandhi, "A survey of structural and multidisciplinary continuum topology optimization: Post 2000," *Struct. Multidisciplinary Optim.*, vol. 49, no. 1, pp. 1–38, Jan. 2014.

[33] G. Sabiston and I. Y. Kim, "3D topology optimization for cost and time minimization in additive manufacturing," *Struct. Multidisciplinary Optim.*, vol. 61, no. 2, pp. 731–748, Feb. 2020.

[34] K. Svanberg, "The method of moving asymptotes—A new method for structural optimization," *Int. J. Numer. Methods Eng.*, vol. 24, no. 2, pp. 359–373, Feb. 1987.

[35] T. Yilmaz, N. Hasan, R. Zane, and Z. Pantic, "Multi-objective optimization of circular magnetic couplers for wireless power transfer applications," *IEEE Trans. Magn.*, vol. 53, no. 8, pp. 1–12, Aug. 2017.

[36] O. Sigmund, "On the usefulness of non-gradient approaches in topology optimization," *Struct. Multidisciplinary Optim.*, vol. 43, no. 5, pp. 589–596, May 2011.

[37] F. Lucchini, R. Torchio, and P. Alotto, "Gradient-informed Pareto-based multi-objective binary topology optimization," *IEEE Access*, vol. 13, pp. 86576–86587, 2025.

[38] F. Wang, B. S. Lazarov, and O. Sigmund, "On projection methods, convergence and robust formulations in topology optimization," *Struct. Multidisciplinary Optim.*, vol. 43, no. 6, pp. 767–784, Jun. 2011.

[39] M. Zucca et al., "Assessment of the overall efficiency in WPT stations for electric vehicles," *Sustainability*, vol. 13, no. 5, p. 2436, Feb. 2021.

[40] H. Zhao et al., "An improved core loss model of ferromagnetic materials considering high-frequency and nonsinusoidal supply," *IEEE Trans. Ind. Appl.*, vol. 57, no. 4, pp. 4336–4346, Jul. 2021.

[41] V. Shevchenko, O. Husev, R. Strzelecki, B. Pakhaliuk, N. Poliakov, and N. Strzelecka, "Compensation topologies in IPT systems: Standards, requirements, classification, analysis, comparison and application," *IEEE Access*, vol. 7, pp. 120559–120580, 2019.

Giulio Poggiana received the M.Sc. degree in electrical energy engineering from the University of Padua, Padua, Italy, in 2023, where he is currently pursuing the Ph.D. degree in electrical engineering.

His research interests include wireless power transfer, electromagnetic modeling and simulation, and induction heating.

Wenjie Yuan received the B.E. degree in automation from Chongqing University, Chongqing, China, in 2018, where he is currently pursuing the Ph.D. degree in control theory and control engineering with the College of Automation.

His current research interests include the standardization and safety design of electric vehicle wireless power transfer systems and power fluctuation suppression in dynamic systems.

Riccardo Torchio (Member, IEEE) was born in Padua, Italy, in 1992. He received the M.S. degree in electrical engineering from the University of Padua, Padua, in 2016, and the dual Ph.D. degree in electrical engineering from the University of Padua and Grenoble Electrical Engineering Laboratory (G2ELab), Université Grenoble Alpes, Grenoble, France, in December 2019.

He is currently with the University of Padua as an Assistant Professor (RTDb). His research interests include numerical methods, optimizations, low-rank compression techniques, uncertainty quantifications, wireless power transfer applications, model order reduction, model predictive control, and the development of integral formulations for the study of low- and high-frequency electromagnetic devices.

Francesco Lucchini received the M.Sc. degree in mathematical engineering from the University of Padua, Padua, Italy, in 2019, and the joint Ph.D. degree in fusion science and engineering from the University of Padua and Ghent University, Ghent, Belgium, in 2023.

He is currently an Assistant Professor (RTDa) at the University of Padua. His research interests include numerical methods, optimizations, and the development of integral formulations for the study of electromagnetic devices.

Vincenzo Cirimele (Senior Member, IEEE) received the M.Sc. (summa cum laude) and Ph.D. degrees in electrical engineering from the Politecnico di Turin, Turin, Italy, in 2013 and 2017, respectively, and the Ph.D. degree in electronics engineering from the Université Paris-Saclay, Gif-sur-Yvette, France, in 2017.

From 2020 to 2021, he was a Technical Responsible with the Research and Development and Innovation Group, Movyon S.p.A., Florence, Italy; and the Autostrade per l'Italia Group, Rome, Italy, where he supervised projects related to energy sustainability and development of highway electric mobility. Since May 2019, he has been among the founders of the start-up Enermove s.r.l., Enermove, Italy, dealing with wireless charging systems for electric vehicles in the industrial field. From 2017 to 2020, he held the position of an Assistant Professor at the Department of Energy, Politecnico di Torino. He is currently an Associate Professor with the Department of Electrical, Electronic, and Information Engineering, University of Bologna, Bologna, Italy. His research interests include technologies for electric mobility, inductive power transmission, electromagnetic modeling and simulation, and power electronics.

Chunsen Tang (Member, IEEE) received the B.S. and Ph.D. degrees from the College of Automation, Chongqing University, Chongqing, China, in 2004 and 2009, respectively.

In 2008, he was a Research Fellow with the Department of Electrical and Computer Engineering, The University of Auckland, Auckland, New Zealand. In 2009, he was with the College of Automation, Chongqing University, where he is currently a Professor. His current research interests include nonlinear modeling and analysis, intelligent control, and wireless power transfer.

Fabrizio Dughiero is a Full Professor of electromagnetic processing of materials (EPM) with the University of Padua, Padua, Italy, where he is also the Chief Scientist with the Laboratory of Electroheat and the Director of the Department of Industrial Engineering. He has been the Founder of the spin-off companies. InovaLab and Unismart Padua Enterprise Ltd., Padua. His current research activity, documented by more than 180 scientific publications, mainly deals with theoretical aspects and applications of EPM and electroheat technologies.

Open Access funding provided by 'Alma Mater Studiorum - Università di Bologna' within the CRUI CARE Agreement